The role of $ZrCl_4$ partial pressure on the growth characteristics of chemical vapour deposited ZrC layers

S Biira[a,b*], PL Crouse[c], H Bissett[d], TT Hlatshwayo[a], EG Njoroge[a], JT Nel[d], TP Ntsoane[d] , JB Malherbe[a]

[a] *Department of Physics, University of Pretoria, Pretoria, 0002 South Africa,*

[b]*Department of Physics, Busitema University P.O Box 236, Tororo Uganda,*

[c]*Department of Chemical Engineering, University of Pretoria, 0002 South Africa*

[d]*The South African Nuclear Energy Corporation (Necsa), Pretoria, 0001 South Africa*

Corresponding Author: Tel.: +27611 894 594, Email address: bsaphina@yahoo.co.uk

Abstract

ZrC layers were deposited in a chemical vapour deposition (CVD) reactor on graphite substrates using a $ZrCl_4$-Ar-CH_4-H_2 precursor mixture. The deposition was conducted at different $ZrCl_4$ partial pressures at a constant substrate temperature of 1400 °C for 2 h at atmospheric pressure. The deposited ZrC layers were characterised using X-ray diffraction (XRD) and field emission scanning electron microscopy (FE-SEM). The effect of $ZrCl_4$ partial pressure on the growth rate, microstructure and surface morphology of the deposited layers was studied. The $ZrCl_4$ partial pressure was manipulated by changing the flow rate of the argon carrier gas through the sublimation chamber. The boundary layer thickness decreased as $ZrCl_4$ partial pressures increased due increased argon flows. The increased $ZrCl_4$ partial pressure increased the growth rate of ZrC layers linearly. It was found that the transport process of the source materials was laminar and forced convection flow. The flow process of source materials through the boundary layer to the reacting surface was also

illustrated using a model. The average crystallite size increased with $ZrCl_4$ partial pressures, whereas the lattice parameter, lattice strain and dislocation density decreased as $ZrCl_4$ partial pressure increased. The surface morphology of the as-deposited ZrC layers varied with the $ZrCl_4$ partial pressure. The size of crystals grew larger and the cavities surrounding them decreased in number and size as the $ZrCl_4$ partial pressure increased.

Keywords: Zirconium carbide; Chemical vapour deposition; Partial pressure; Surface morphology; Microstructure, Growth rate.

1   Introduction

The properties and importance of ZrC either as a layer or bulk material have already been emphasised by several authors [1−7]. Of particular interest for our research group and hence for this study is its proposed usage for coating the zircaloy cylinders containing the fuel elements in conventional nuclear reactors and in high-temperature gas cooled nuclear reactors [5]. ZrC, either as a powder mixed with the fuel or as a thin layer on the UO_2 fuel kernel has been proposed for use as an oxygen getter in TRISO (tristructural-isotropic) fuel particles. Due to its high oxidation potential, ZrC is perceived to act as a reducing agent for the oxygen generated from the UO_2 fission process [8,9]. This may prevent unfavourable oxidation reactions and reduce the formation of CO both of which are detrimental, especially at high fuel burn-up levels [2,8]. ZrC has also been proposed as a possible replacement for the SiC layer as a diffusion barrier layer for containing fission products in the TRISO fuel particle [5]. This is because ZrC has a low neutron capture cross section, enhanced resistance to fission products attack and diffusion, and is stable even at high temperatures [8]. However, the properties of ZrC layer vary greatly depending on synthesis technique used and how well the deposition parameters are managed during its production.

Chemical vapour deposition (CVD) compared to other ZrC synthesis techniques has been highlighted as a method of choice to grow good quality layers [2,10]. CVD enables the production of relatively pure uniform layers with good adhesion and reproducibility at fairly good deposition rates [11,12]. The growth and structure of layers deposited by CVD vary depending on the reactor geometry (size and type of the reactor, inlet-substrate gap, inlet diameter) and deposition parameters. The deposition parameters include temperature, time, reactor total pressure and the precursor's properties (i.e. type, compositions, concentrations, flow rates and partial pressures) [13,14]. The structure of the chemical vapour deposited layer determines its physical properties. Therefore, the CVD parameters, especially those that affect the layer structure, should be studied carefully and optimised. The layer structure and growth are mainly controlled by the substrate temperature and the gas concentrations in the reaction chamber [10,15]. The inlet gas concentration is primarily regulated by the partial pressure of the precursors. The partial pressure of a gas determines its thermodynamic activity. It has been noted that gases will diffuse, react or dissolve according to their partial pressures, and not necessarily according to their concentrations in a gas mixture [16]. In a CVD reactor, the partial pressure depends on gas flow rates, vapourising temperature, and substrate-gas inlet gap. The influence of substrate-inlet gap on the growth characteristics of ZrC layers has been reported in [13]. Several researchers have studied the effect of the carbon source (especially CH_4 and C_3H_6) [14,17,18] and hydrogen flow rates [17,19] on the properties of ZrC layers. The effect of reactor total pressure on the growth and structure of ZrC layers has also been reported by Zhu *et al*. [17]. However, to our knowledge, no study has been reported on the effect of $ZrCl_4$ partial pressure on the growth and structure of ZrC grown by thermal CVD. $ZrCl_4$ was chosen for this study since it is more commonly used for CVD of ZrC layers than the other halides such as ZrF_4, $ZrBr_4$ and ZrI_4. This is due to the fact that $ZrCl_4$ is the most volatile of the zirconium halides; it is less dangerous than $ZrBr_4$ and ZrC with a better stoichiometry can be obtained more effectively than when using ZrI_4 [19]. Therefore, this

study reports on the investigation of the influence of the $ZrCl_4$ partial pressure on the growth rate, microstructure and surface morphology of deposited ZrC layers on graphite substrates.

## 2   Experimental procedure

ZrC layers were grown on graphite substrate disks (radius 10 mm, thickness 2.5 mm) by reacting $ZrCl_4$, CH_4 and H_2 in an in-house built vertical-wall CVD reactor at atmospheric pressure (87 kPa absolute at location). The reaction chamber, a graphite tube, with 2.5 cm internal diameter (d) was inductively heated by a copper coil connected to a 10 kW RF power supply. The gap between the substrate and the gas inlet (X) was maintained at 90 mm. Figure 1 shows the experimental set-up for the reactor system. The gas flow rates were monitored by well-calibrated rotameters. Exit gases from the reactor were directed through a $CaCO_3$ scrubber fitted before the vacuum pump and subsequently through the extraction ventilation. The system was purged with argon before the start of each experimental run. To attain thermal equilibrium stability, the reaction chamber was allowed to heat up for 10 minutes before the start of the 2 h deposition. ZrC layers were deposited at a substrate temperature of 1400 °C. At the end of the 2 h, all the inlet gases were closed and the reactor was allowed to cool to room temperature before removing the deposited samples. In fact, layers that were removed before the reactor cooled completely to room temperature were found to have several cracks and were not used for analysis in this study. The substrates were weighed before and after deposition to estimate the mass gain. The average growth rate of the ZrC layers was calculated from the mass gain, the surface area of the substrate and theoretical density of ZrC (6.59 g/cm^3).
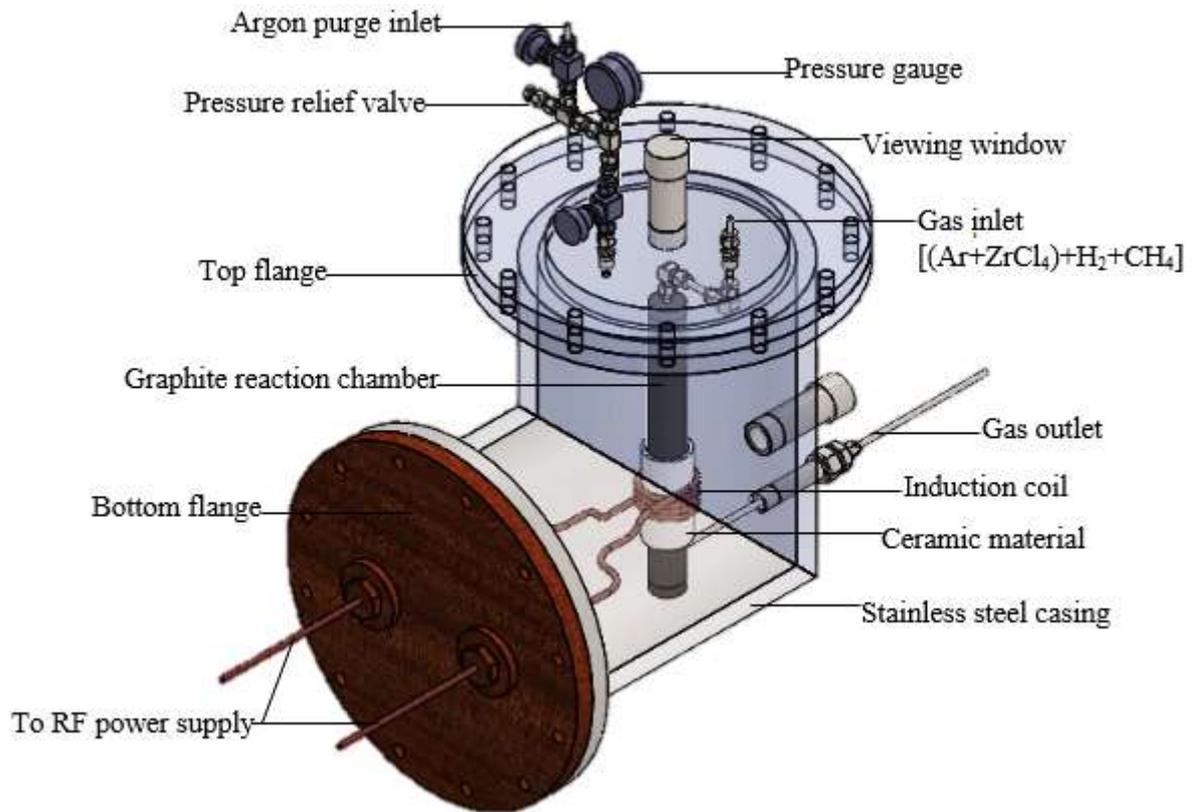
Figure 1: The CVD reactor set-up.

During the experimental run, $ZrCl_4$ powder was housed in a stationary stainless steel vaporiser at a uniform temperature of 300 °C. To avoid agglomeration of the $ZrCl_4$ powder, the $ZrCl_4$ delivery line to the reactor was also maintained at 300 °C by electric heat tracing tape. The vapour pressure of $ZrCl_4$ was determined from the vapour pressure – temperature calibration curve given in Figure 2. The partial pressure of $ZrCl_4$ was controlled by controlling the argon flow rate and the temperature of the vaporiser. From Figure 2, a temperature of 300 °C corresponds to a $ZrCl_4$ vapour pressure of about 43 kPa. The $ZrCl_4$ mass flow rate in the argon carrier gas was determined from the quantity of $ZrCl_4$ swept from the vaporiser during each experimental run.
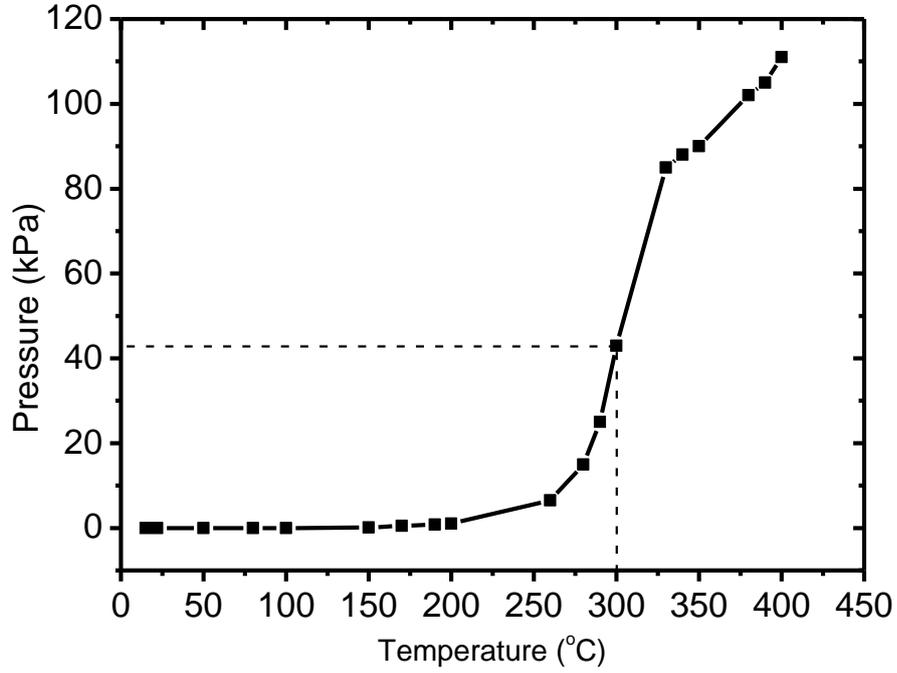
Figure 2: *Variation of ZrCl₄ vapour pressure with temperature.*

By applying Dalton's law of partial pressure given in Equation (1), Amagat's law of partial volume given in Equation (2), and the ideal gas equation we obtain, the pressure, volume and the mole amount relation given by equation (3) [20,21].

$$P_T = \sum_{i=1}^{n} P_i \tag{1}$$

$$V_T = \sum_{i=1}^{n} V_i \tag{2}$$

$$\frac{V_i}{V_T} = \frac{P_i}{P_T} = \frac{n_i}{n_T} \tag{3}$$

Here V_i is the partial volume and P_i is the partial pressure of any individual gas component i, P_T is the total pressure of the gas mixture, n_i is the mole amount of substance of gas i, n_T is the total number of moles in the gas mixture.

For steady state conditions (i.e. where the total volume, total the pressure and the deposition temperature are all constant), then the partial pressure can be written in terms of the volumetric flow rates of the gases

6

$$\frac{P_i}{P_T} = \frac{\Delta V_i / \Delta t}{\Delta V_T / \Delta t} = \frac{\dot{V}_i}{\dot{V}_T} \qquad (4)$$

The partial pressure fraction of $ZrCl_4$ (i.e. P_{ZrCl_4}/P_T) was calculated from Equation (5) in which the volumetric flow rate, $\dot{V}_{ZrCl_4}$ of $ZrCl_4$ was determined from Equation (6).

$$\frac{P_{ZrCl_4}}{P_{Total}} = \frac{\dot{V}_{ZrCl_4}}{\dot{V}_{Ar} + \dot{V}_{ZrCl_4} + \dot{V}_{H_2} + \dot{V}_{CH_4}} \qquad (5)$$

$$\dot{V}_{ZrCl_4} = \frac{\dot{m}RT_V}{MP_V} \qquad (6)$$

From Equation (6), $\dot{m}$ is the mass flow rate of $ZrCl_4$, M is the molar mass of $ZrCl_4$, R is the universal gas constant, T_V is the temperature of the vaporiser and P_V is the vapour pressure of $ZrCl_4$ in the stream of inlet gases. Table 1 gives the deposition conditions.

Table 1: Deposition parameters and gas properties

Experiment number	1	2	3	4	5
Gas flow rates					
CH_4 (sccm)	15	15	15	15	15
H_2 (sccm)	853	853	853	853	853
Ar (sccm)	264	415	562	704	849
$ZrCl_4$ (g/h)	0.64	0.81	0.98	1.14	1.34
$ZrCl_4$ (sccm)	5.07	6.42	7.77	9.04	10.38
$ZrCl_4$ partial pressure fraction ($\times 10^{-3}$)	4.45	4.98	5.40	5.72	6.01
Gas at 300 °C	**CH_4**	**H_2**		**Ar**	
Viscosity $\times 10^{-5}$ (Ns/m^2)	1.883	1.353		3.67	
Density (kg/m^3)	0.337	0.042		0.8494	

2.1 Characterisation

The structure analysis of ZrC layers deposited at the selected constant temperature of 1400 °C for different $ZrCl_4$ partial pressures was carried out using a Bruker XRD D8 Advance with a Cu K_α radiation source (λ=1.5406 Å). During XRD pattern collection the working potential and current were set at 40 kV and 40 mA respectively. The values of 2θ were recorded between 15° to 125°. The surface morphology of the layers was characterised using a Zeiss

Ultra Plus Field Emission Scanning Electron microscopy (FE-SEM) at an acceleration voltage of 1 kV.

The graphite substrates were weighed by an electronic mass balance with a precision of 0.0001 g prior to and after deposition to determine the weight gain. Using a ZrC density of 6.59 g/cm^3, the measured weight gain, and with a known value of the surface area, the average layer growth rate (thickness per deposition time) was calculated at the various partial pressures of $ZrCl_4$.

3 Results and discussion

3.1 Gas flow behaviour and qualitative description of the deposition process

The flow behaviour of the gases in the reaction chamber was established by calculating the magnitudes of the following dimensionless quantities. They were the Grashof number, *Gr* and the Reynolds number, *Re*. The values of these quantities given in Table 2 were calculated using Equations (7) and (8) [21–23].

$$Gr = \frac{g\rho^2 d^3 \Delta T}{T_o \eta^2} \tag{7}$$

$$\mathrm{Re} = \frac{dv\rho}{\eta} \tag{8}$$

where ΔT is the temperature difference between the reactor wall and the substrate and T_o is the temperature of the gases as it enters the reactor. The gas flow was found to be laminar (i.e. $Re < 1000$ [23]) and forced convection dominated (i.e $Gr/Re^2 < 10$ [23]). The boundary layer thickness δ was also calculated from $\delta = \sqrt{\dfrac{Xd}{\mathrm{Re}}}$, where $d = 25$ mm is the diameter of the reaction chamber and $X = 90$ mm is substrate-gas inlet gap.

The velocity *v*, density ρ and viscosity η of the mixture of gases entering the reaction chamber were calculated using equations (9), (10) and (11) [21] respectively.

$$v = \frac{\sum_i \rho_i v_i}{\sum_i \rho_i} \qquad (9)$$

$$\rho = \frac{\sum_i \rho_i \dot{V}_i}{\sum_i \dot{V}_i} \qquad (10)$$

$$\eta = \frac{\sum_i y_i \eta_i \sqrt{M_i}}{\sum_i y_i \sqrt{M_i}} \qquad (11)$$

where ρ_i, v_i, y_i, M_i, and η_i, are the density, velocity, mole fraction, molar weight and viscosity respectively of the ith gas component at the desired temperature given in Table 1. $v_i = \dot{V}_i / (60\pi r^2)$ and r (0.32 cm) is the radius of the inlet feed line. The mole fraction of an individual gas was determined from their volumetric flow rates as $y_i = \dot{V}_i / \sum_i \dot{V}_i$ [21].

In an attempt to increase the $ZrCl_4$ partial pressures, the argon flows were increased which improved the overall mean flow velocity of the reactants. Therefore this increased argon flows (and hence increase in the overall mean flows) decreased the boundary layer thickness (see Figure 3), consequently increasing the arrival rate (the flux) of the reactants. The boundary layer thickness was found to decrease from 9.6 mm to 4.5 mm as the $ZrCl_4$ partial pressure fraction increase from 4.45×10^{-3} to 6.01×10^{-3}.

Table 2: Gas flow parameters and dimensionless quantities.

Experiment #	1	2	3	4	5
Partial pressure fraction $\times 10^3$	4.45	4.98	5.4	5.72	6.01
v (cm/s)	11.2	16.6	21.9	27.0	32.2
ρ (kg/m^3)	0.234	0.307	0.363	0.407	0.444
$\eta \times 10^{-5}$ (Ns/m^2)	2.618	2.921	3.065	3.160	3.231
Re	24.5	43.6	64.7	86.7	110.5
$\delta \times 10^{-3}$ (m)	9.6	7.2	5.9	5.1	4.5
$Gr \times 10^3$	2.1	3.0	3.7	4.4	5.1
Gr/Re^2	3.4	1.6	0.9	0.6	0.4
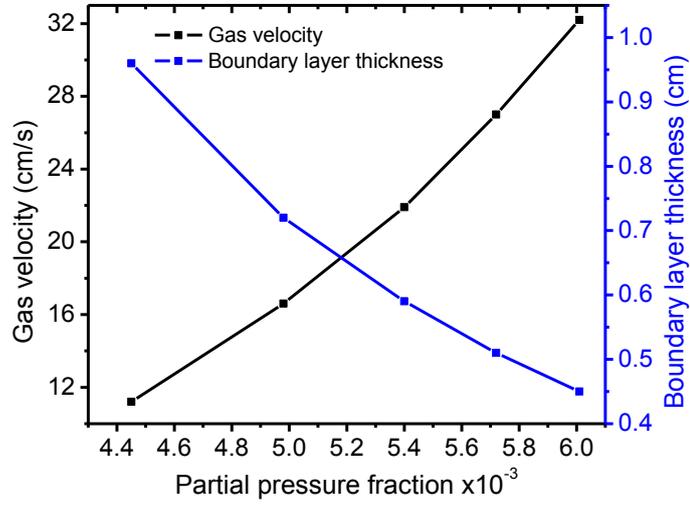
Figure 3: Variation of boundary layer thickness and mean gas velocity with $ZrCl_4$ partial pressure fraction

The inlet gas stream was considered to be an ideal gas that was being transported through a boundary layer to the deposition surface. By applying Fick's law, the diffusion of $ZrCl_4$ vapour from the bulk gas stream towards the substrate may be described by the flux J_1 given

by; $J_1 = \dfrac{-D}{RT}\dfrac{dp_{ZrCl_4}}{dx}$. In our case, this equation can be approximated by $J_1 = \dfrac{D}{RT}\dfrac{p_b - p_s}{\delta}$,

where p_b is the partial pressure fraction of $ZrCl_4$ in the gas bulk stream, p_s is the partial pressure fraction of $ZrCl_4$ at the substrate surface, and T is the deposition temperature [15,24,25]. It is important to note that the $ZrCl_4$ concentration C_{ZrCl_4} is related to its partial

pressure p_{ZrCl_4} by $C_{ZrCl_4} = \dfrac{p_{ZrCl_4}}{RT}$.

After crossing the boundary layer, the gases arrive at the substrate surface. On arrival, the active gases $ZrCl_4$ and carbon containing species are adsorbed onto the substrate and react

forming a layer. The flux J_2 consumed by the reacting surface may be given by $J_2 = \dfrac{k_m}{RT}p_s$,

where k_m is the surface reaction rate constant [15]. For the sake of establishing p_s, we assumed a steady state condition where the mass flux crossing the boundary layer was equal to the flux consumed at the substrate surface to form a layer (i.e. $J_1 = J_2$). So that
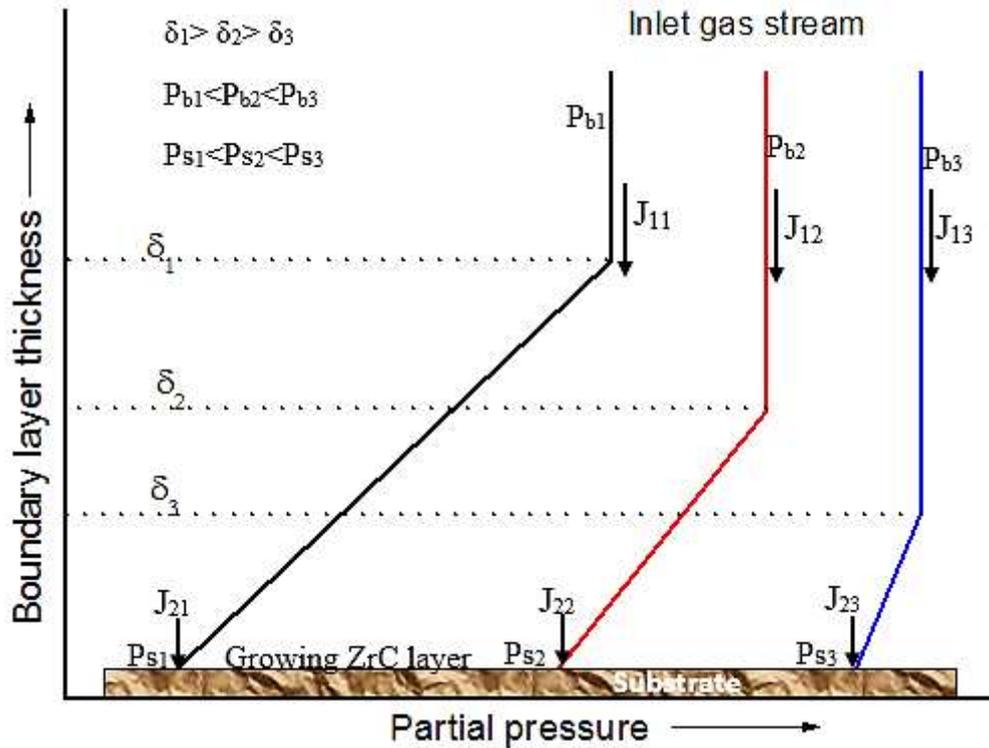
10

$$p_s = \frac{\frac{D}{\delta} p_b}{\left(\frac{D}{\delta} + k_m\right)}.$$ It has already been established from previous studies that at the current

growth conditions, the deposition of ZrC is mass transport lilmited [13][26]. In this case

$\frac{D}{\delta} << k_m$, so that $p_s \approx \frac{D}{\delta k_m} p_b$ [12,15]. This means that $p_s < p_b$. Therefore the gas transport

across the boundary layer for this deposition process may schematically be presented as

shown in Figure 4.

Figure 4: *Schematic of the CVD reactant transport model across the boundary layer. P_{b1}, P_{b2}, P_{b3} are the partial pressures at the inlet and Ps_1, Ps_2, Ps_3 are their corresponding partial pressures at the surface. Also J_{11}, J_{12} J_{13} are the diffusion fluxes of the gas at the inlet and J_{21}, J_{22}, J_{23} are the corresponding fluxes close to the substrate surface.*

3.2   Effect of ZrCl$_4$ partial pressure on ZrC growth rate

To establish the dependence of ZrC layers growth rate on the ZrCl$_4$ partial pressure, the

growth rate of ZrC layers deposited at 1400 °C was plotted against the ZrCl$_4$ partial pressure

as indicated in Figure 5. This plot shows that, within experimental error, the growth rate of

11

ZrC layers increased linearly with $ZrCl_4$ partial pressure. As indicated in Section 3.1, mass transport limits the deposition such that the flux arriving at the substrate is proportional to the rate of chemical reaction of the reacting species at the substrate interface. The flux J_2, which is proportional to the rate of chemical reaction of the reactants on the growing surface (resulting from partial pressures), and the growth rate k of the layer are related by $k = v_k J_2$, where v_k is the molecular volume of the crystal [15]. This explains the linear growth rate of the layers with partial pressure, and is in agreement with Figure 4.
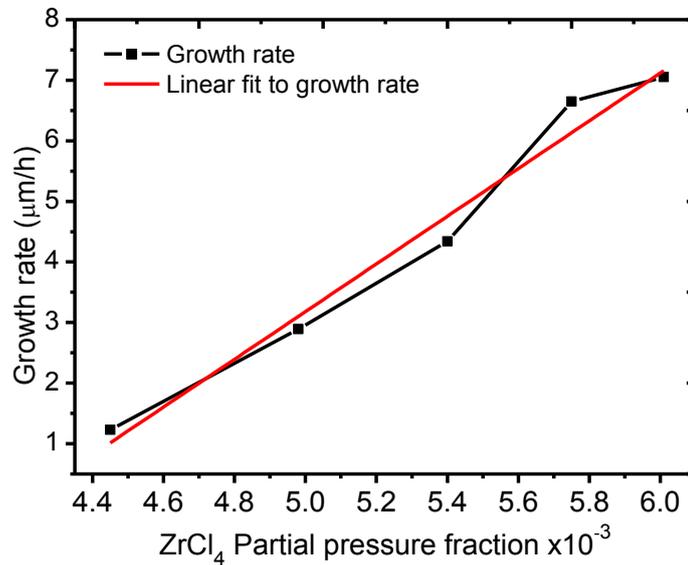
Figure 5: Effect of ZrCl₄ inlet partial pressure fraction on growth rate.

Another aspect accounting for the variation of growth rate with partial pressure is the concentration of the reacting species in the gas mixture. At low $ZrCl_4$ partial pressures, there are more carbon-containing species than zirconium containing species in the reaction chamber which accounts for the low ZrC growth rate. This is due to the fact that the growth rate of ZrC layers was limited by the availability of Zr-containing species. Therefore any increase in $ZrCl_4$ partial pressure boosted the ZrC layer growth rate. For further illustration, an HSC Chemistry software (an equilibrium thermodynamics chemical software program) [27] was used to study the behaviour of the reacting species. Figure 6 shows the $ZrCl_4$ dependence speciation curve for the $ZrCl_4$-CH_4-H_2 system. According to Figure 6, at a deposition

12

temperature of 1400 °C, the methane gas was fully decomposed to carbon and hydrogen while $ZrCl_4$ remained in its gaseous form. So there was always an excess of carbon and therefore at low $ZrCl_4$ partial pressures (like those used in this study) the reaction between the active species is zirconium limited.
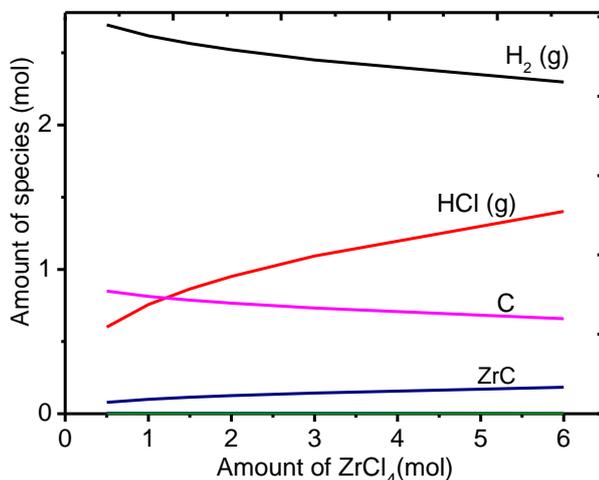
Figure 6: *$ZrCl_4$ concentration dependence speciation curve for $ZrCl_4$-CH_4-H_2 feed system at 1400 °C.*

3.3 Microstructural analysis

Figure 7 shows the XRD patterns of ZrC layers deposited at 1400 °C for different $ZrCl_4$ partial pressures. For confirmation purposes, the diffraction patterns were matched with the standard ICDD (International Centre for Diffraction Data Release 2007) file numbers ZrC: 03-065-8833 and C: 00-008-0415. Ten reflections (111), (200), (220), (311), (222), (400), (331), (420), (422) and (511) corresponding to 2θ° at about 32.9, 38.3, 55.2, 65.9, 69.2, 81.9, 91.2, 94.3, 106.8 and 116.8 respectively are indicated in Figure 7. The ZrC peaks present were indexed within a cubic rock-salt (NaCl) structure type.
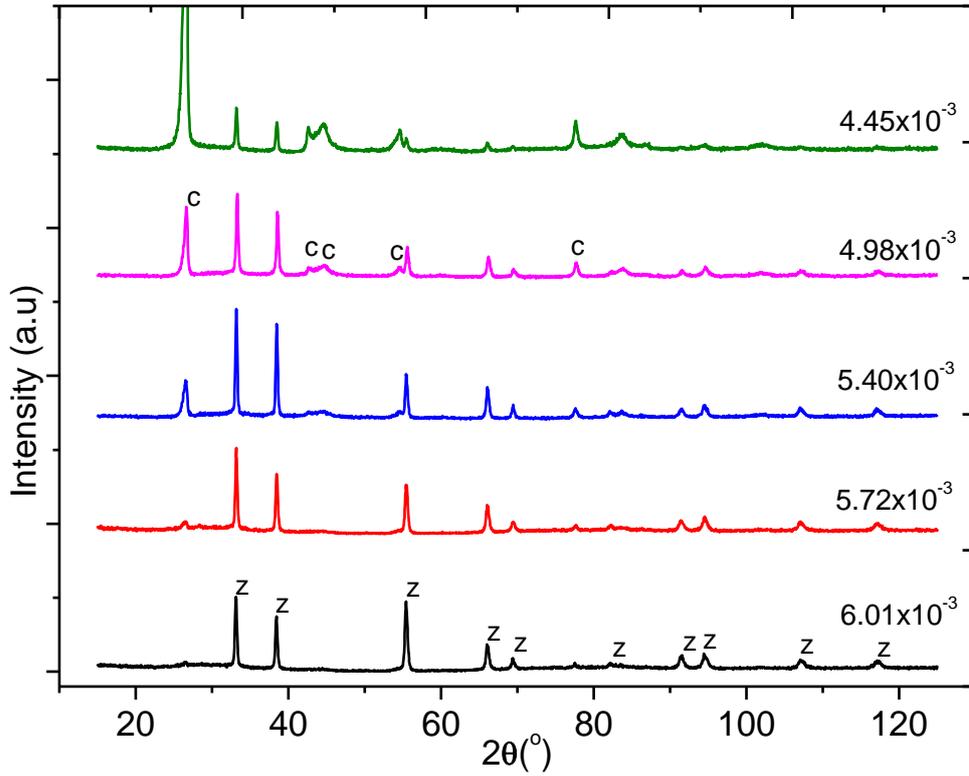
Figure 7: XRD patterns of ZrC layers deposited at 1400 °C for different ZrCl$_4$ partial pressure fractions.

The carbon phase present was hexagonal graphite with its reflections (hkil) of (0002), (10$\bar{1}$0), (10$\bar{1}$1), (10$\bar{1}$2), (0004), (10$\bar{1}$3), (11$\bar{2}$0), (11$\bar{2}$2), (0006), (20$\bar{2}$1) and (11$\bar{2}$4) at 2θ° at about 26.5, 42.4, 44.6, 50.7, 54.9, 60.0, 77.5, 83.5, 87.1, 94.1 and 101.8 respectively. In Figure 7 only the most prominent carbon peaks are indicated by c. The intensities of the carbon peaks increased with a decrease in ZrCl$_4$ partial pressure. The decrease in concentration of ZrCl$_4$ vapour as the partial pressure was reduced, resulted in excess carbon (from the decomposition of methane) which was deposited as free carbon alongside ZrC. As illustrated in Figure 6, all of the methane gas was decomposed into H$_2$ and carbon while the ZrCl$_4$ vapour remained in gaseous form throughout the experimental run [14]. The amount of carbon from methane was normally higher than ZrCl$_4$ (see Table 1) and therefore leading to C being deposited alongside ZrC.

14

The preferred orientation as determined from the texture coefficient calculated using the Harris method [28,29] was found to vary with $ZrCl_4$ partial pressure. At the lowest $ZrCl_4$ partial pressure fraction of 4.45×10^{-3}, the (111) diffraction plane was the preferred orientation. When $ZrCl_4$ partial pressure fraction increased to 4.98×10^{-3} and 5.40×10^{-3}, the preferred orientation shifted to (200) and finally at higher partial pressure fractions of 5.72×10^{-3} and 6.01×10^{-3}, the preferred orientation changed to (220). This is due to the growth competition among different crystal planes occurring during deposition because of the differences in surface energies and/or growth anisotropies. At low $ZrCl_4$ partial pressures, the arrival rate of Zr atoms at the growing surface is low enough for equilibrium crystal growth conditions to be achieved. Therefore, one would expect the planes with the minimum surface energy to grow preferentially compared to those with high surface energies, thereby minimising the Gibbs free energy of the crystallites, in accordance with Wulff's law [30]. Among all the ZrC planes, the (111) diffraction plane has the lowest surface energy, because of the fact that its surface atoms are the most densely packed per unit area. Higher indices planes are difficult to form because they have relatively long Zr-C distances. As the $ZrCl_4$ partial pressure was increased, the higher arrival rate of $ZrCl_4$ atoms at the substrate surface resulted in increased atomic collisions and, thus, interacting molecules which allowed for non-equilibrium crystal growth to take place. This implies that the high-index crystallographic planes (200) and (220) also formed.

3.3.1 Lattice parameter, lattice strain and residual stress

The lattice parameters (*a)* of the ZrC layers were determined from the Miller indices (hkl) and interplanar spacing d of the various planes [28] using Equation (12).

$$a = d \Big/ \sqrt{\left(h^2 + k^2 + l^2\right)} \tag{12}$$

The lattice parameter values obtained by this method were found to vary from one diffraction plane to another for the same sample. Therefore, Nelson-Riley plots were used to determine

the corrected lattice parameter value for each ZrC deposited layer. Nelson-Riley plots are plots of the lattice parameter calculated from Equation (12) and the error function $f(\theta)$ calculated from Equation (13) [31].

$$f(\theta) = \frac{1}{2}\left(\frac{\cos^2\theta}{\sin\theta} + \frac{\cos^2\theta}{\theta}\right) \tag{13}$$

The intercept of Nelson-Riley plots (i.e. at $\theta=90$) gives the corrected value of the lattice parameter of a particular sample. The Nelson-Riley plots are not shown in this paper. The corrected lattice parameter values obtained from the plots decreased from 4.6995 Å to 4.6938 Å with an increase in the $ZrCl_4$ partial pressure from 4.45×10^{-3} to 6.01×10^{-3} (see Figure 8). This observation may be due to the presence of defects in the ZrC layer at low $ZrCl_4$ partial pressures. At low partial pressure, there are more carbon inclusions in the lattice as illustrated in Figure 7. The carbon inclusions in the lattice of the ZrC layers are reduced when the $ZrCl_4$ partial pressure is increased. The reduction in the carbon inclusions in the ZrC layer might have led to lattice contraction which then resulted in a reduced lattice parameter value. This might be due to the presence of carbon impurities increasing the distance between the neighbour atoms in the ZrC lattice structure. This gives rise to relaxation of the lattice causing the lattice parameter to increase.
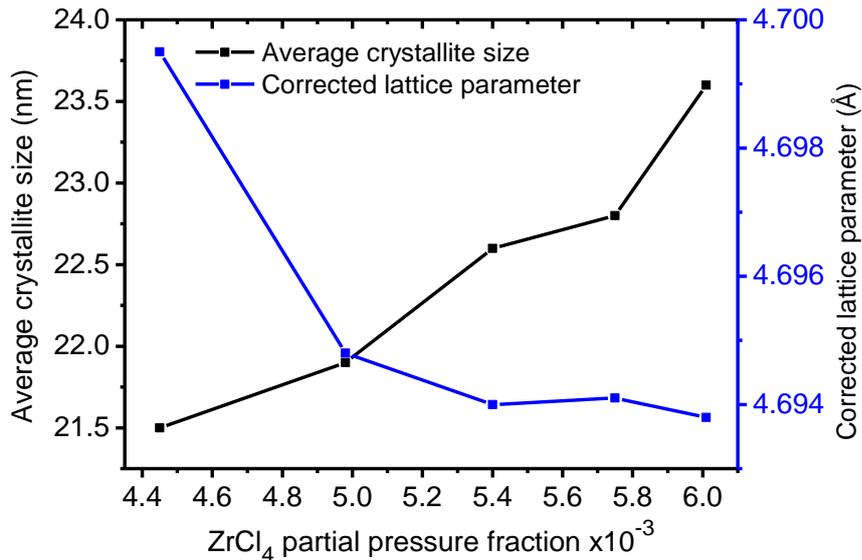

Figure 8: *Influence of ZrCl₄ partial pressure on average crystallite size and lattice parameter.*

16

All the corrected lattice parameter values of the as-deposited ZrC layers were found to possess lattice parameter values that are within the range of the ZrC bulk material (4.6890–4.7017 Å [1,32–34]). However, it is important to note that, layers deposited by this method, always experience some kind of strain [35] and this may be the reason for any variation of the lattice parameter value from the "actual expected value". Strain (ε) measures the level of distortions and crystal imperfections in the material and was calculated from peak broadening B at half width at full maximum and diffraction angle θ [36] as indicated by Equation (14).

$$\varepsilon = \frac{B}{4\tan\theta} \tag{14}$$

There was a decrease in lattice strain from 4.08×10^{-3} to 3.72×10^{-3} as the ZrCl$_4$ partial pressure was increased from 4.45×10^{-3} to 6.01×10^{-3} as shown in Figure 9. This is because when the ZrCl$_4$ partial pressure was increased the concentrations of the defects (e.g. carbon inclusions) in the as-deposited ZrC layer reduced which resulted in a reduction in the lattice strain. Also when the layer thickness increased due to an increase in partial pressure, the influence of the substrate on the layer is reduced this in turn also reduces the strain in the grown layer.
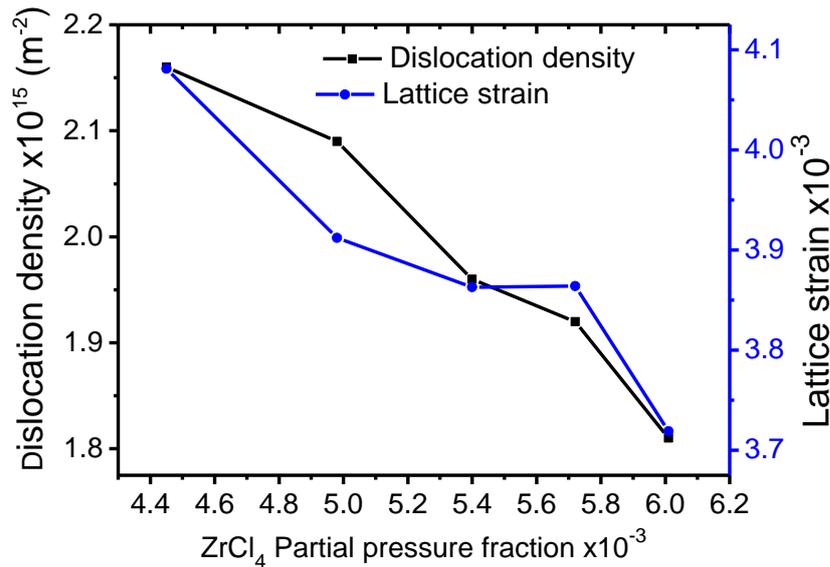
Figure 9: Variation of dislocation density and lattice strain with ZrCl$_4$ partial pressure fraction.

3.3.2 Average crystallite size and dislocation density

The average crystallite size G of ZrC layers deposited at different $ZrCl_4$ partial pressure was determined from Scherrer's formula [37] given by Equation (15).

$$G = \frac{0.94\lambda}{B\cos\theta} \tag{15}$$

where λ is the X-rays wavelength (0.15418 nm). The effect of instrumental broadening was subtracted from the XRD profile before calculating the values of crystallite sizes. The values of average crystallite size changed from 21.5 nm to 23.6 nm as the $ZrCl_4$ partial pressure fraction changed from 4.45×10^{-3} to 6.01×10^{-3}, as can be seen from Figure 8. As shown in Figure 6, methane decomposes into carbon and hydrogen long before the decomposition of $ZrCl_4$. Therefore at low $ZrCl_4$ partial pressures, carbon is in excess of Zr-containing species and carbon may even deposit first on the substrate before ZrC could deposit. The presence of this free carbon will restrict the ZrC crystal growth and crystallisation process. The thermodynamics and kinetics involving ZrC deposition are different from those involving ZrC+C, so are their nucleation and growth mechanisms. When the $ZrCl_4$ partial pressure was increased the Zr-containing species combining with the carbon containing species increased, consequently reduced the amount of free carbon in the layer. Reducing the amount of the free carbon reduced its interference to the ZrC crystal growth which resulted in increased crystallite size.

Assuming a random distribution of dislocations, the number of dislocation lines crossing a unit area in the layer of the deposited ZrC (here referred to as dislocation density L was calculated from Williamson-Smallman's formula [38] [39] given by Equation (16).

$$L = \frac{1}{G^2} \tag{16}$$

where G is the average crystallite size. Dislocation density is one of the indications of the number of defects in the layer and it was found to vary from 2.16×10^{15} m^{-2} to 1.81×10^{15} as the partial pressure fraction varied from 4.45×10^{-3} to 6.01×10^{-3} (see Figure 9).

It is evident from Figure 9 that as the partial pressure increased, the lattice strain and the dislocation density decreased. This may be attributed to the reduction in carbon inclusions which can give rise to extended defects such as dislocations.

3.4 Surface morphology analysis

Figure 10 shows in-lens SEM images of ZrC layers deposited at 1400 °C for different ZrCl$_4$ partial pressures. At the low ZrCl$_4$ partial pressure fraction of 4.45×10^{-3} (Figure 10 (a)), the layer had small particles tending to cluster together surrounded by lots of voids. As the ZrCl$_4$ partial pressure increased, there was increased aggregation of the particles. This resulted in a decrease in both the size and number of voids in the ZrC layer causing the layer to become increasingly homogeneous. The ZrC layer coverage of the substrate surface was also enhanced. At the ZrCl$_4$ partial pressure fraction of 6.01×10^{-3} (Figure 10(e)), almost all the clusters joined together and the voids significantly reduced. There was no distinctive change in the shape of the crystals as the partial pressure was varied. In line with the average crystallite size as determined by XRD (see Figure 8), the particles in the SEM images also increased in size with increasing ZrCl$_4$ partial pressure. There was an increased tendency of clusters growing on top of each other and whose sizes also increased with the increase in ZrCl$_4$ partial pressure. It can be deduced that the layer surface grew by both additions of atoms and coalescence of primary particles since particles tend to pile on top of the other and also merge as they increase in size.
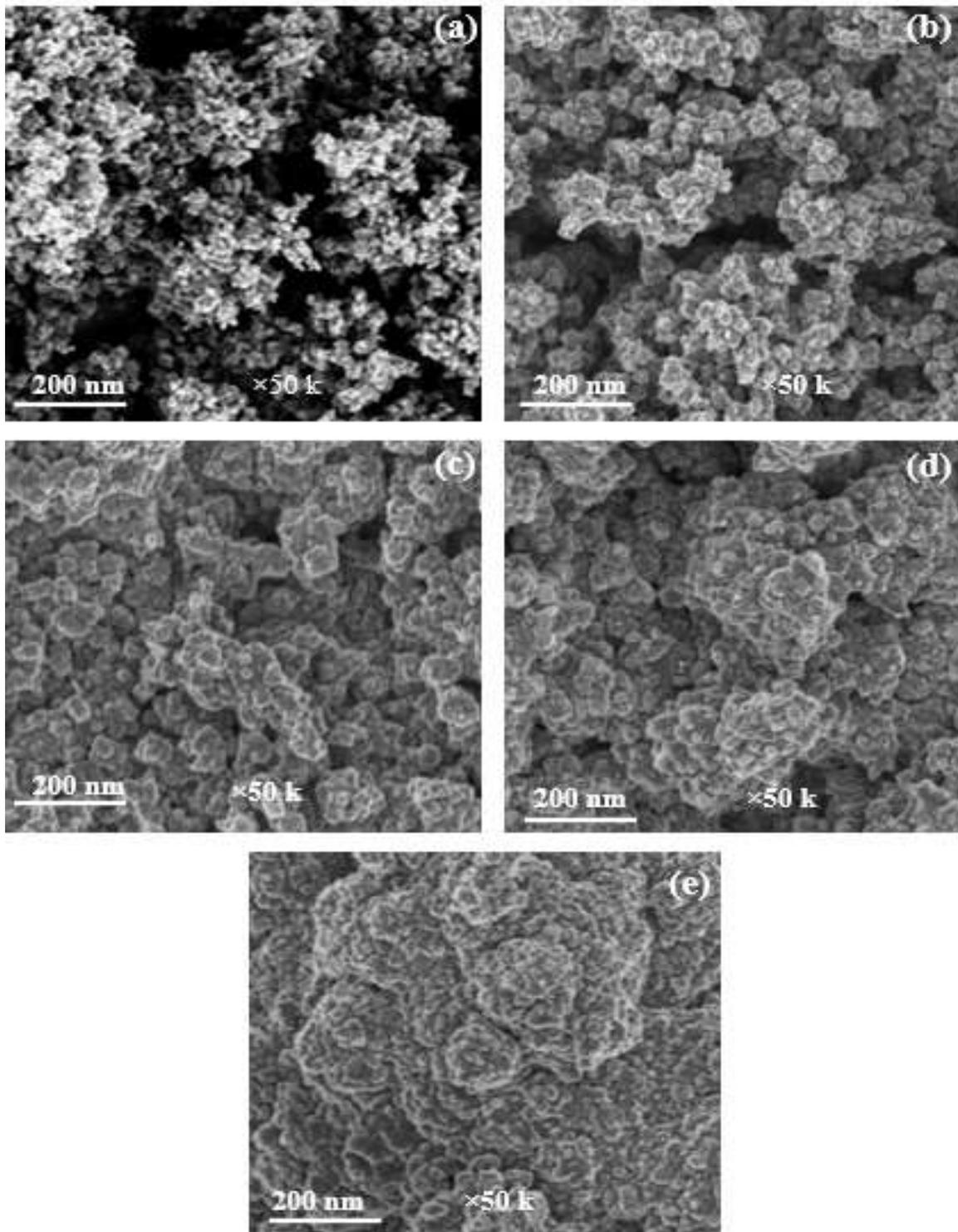
Figure 10: *FE-SEM images of ZrC layers deposited at 1400 °C for different ZrCl$_4$ partial pressure fractions: (a) 4.45×10^{-3}; (b) 4.98×10^{-3}; (c) 5.40×10^{-3}; (d) 5.72×10^{-3}; (e) 6.01×10^{-3}.*

4 Conclusion

ZrC layers were successfully deposited on graphite substrates in a vertical CVD reactor. The growth rate of ZrC layers was studied at various ZrCl$_4$ partial pressures. The role of ZrCl$_4$ partial pressure on the microstructure and surface morphology was investigated using XRD

and FE-SEM. The boundary layer thickness decreased resulting from increased argon flows. As determined by Reynolds and Grashof numbers, the gas flow process was dominated by laminar and forced convection flows. The transport process of the source materials through the boundary layer to the reacting surface was illustrated using a model. The growth rate of the ZrC layers increased linearly with increasing $ZrCl_4$ partial pressure. The ZrC layer microstructure and morphology varied with $ZrCl_4$ partial pressure. XRD results showed the formation of only the ZrC phase at $ZrCl_4$ partial pressure fractions of 5.72×10^{-3} and 6.01×10^{-3}. As the $ZrCl_4$ partial pressure decreased carbon peaks started to emerge. The carbon peaks were very prominent at the lowest $ZrCl_4$ partial pressure values. The (111) diffraction plane was a more favoured orientation at lower $ZrCl_4$ partial pressure whereas the (200) and (220) were more favoured planes at higher $ZrCl_4$ partial pressure. There was a general increase in average crystallite size with increasing $ZrCl_4$ partial pressure. The lattice parameter, lattice strain and dislocation density decreased with increasing $ZrCl_4$ partial pressure. At low $ZrCl_4$ partial pressures, the ZrC layer had small crystals tending to cluster together surrounded by lots of voids. When the $ZrCl_4$ partial pressure was further increased the crystals increased in size and became more dense and coarse. The clustering and aggregating of particles into big agglomerates were also enhanced as the $ZrCl_4$ partial pressure increased.

Acknowledgements

References

[1]   H.O. Pierson, Handbook of Refractory Carbides & Nitrides: Properties, Characteristics, Processing and Apps., Noyes Publications, New Jersey, 1996.

[2]   Y. Katoh, G. Vasudevamurthy, T. Nozawa, L.L. Snead, Properties of zirconium carbide for

nuclear fuel applications, J. Nucl. Mater. 441 (2013) 718–742.

[3]   Y. Yang, C.A. Dickerson, H. Swoboda, B. Miller, T.R. Allen, Microstructure and mechanical properties of proton irradiated zirconium carbide, J. Nucl. Mater. 378 (2008) 341–348. doi:10.1016/j.jnucmat.2008.06.042.

[4]   Y.S. Won, V.G. Varanasi, O. Kryliouk, T.J. Anderson, L. McElwee-White, R.J. Perez, Equilibrium analysis of zirconium carbide CVD growth, J. Cryst. Growth. 307 (2007) 302–308.

[5]   J.B. Malherbe, Diffusion of fission products and radiation damage in SiC, J. Phys. D. Appl. Phys. 46 (2013) 27.

[6]   T.M. Besmann, R.E. Stoller, G. Samolyuk, P.C. Schuck, S.I. Golubov, S.P. Rudin, J.M. Wills, J.D. Coe, B.D. Wirth, S. Kim, others, Modeling Deep Burn TRISO particle nuclear fuel, J. Nucl. Mater. 430 (2012) 181–189.

[7]   K. Sawa, S. Ueta, Research and development on HTGR fuel in the HTTR project, Nucl. Eng. Des. 233 (2004) 163–172.

[8]   L.L. Snead, Y. Katoh, S. Kondo, Effects of fast neutron irradiation on zirconium carbide, J. Nucl. Mater. 399 (2010) 200–207.

[9]   A. Motta, K. Sridharan, D. Morgan, I. Szlufarska, Understanding the Irradiation Behavior of Zirconium Carbide, Washington D.C, 2013.

[10]   A.C. Jones, M.L. Hitchman, Chemical Vapour Deposition - Precursors, Processes and Applications, Royal Society of Chemistry, London, 2009.

[11]   K.L. Choy, Chemical vapour deposition of coatings, Prog. Mater. Sci. 48 (2003) 57–170.

[12]   P.M. Martin, Handbook of deposition technologies for films and coatings: science, applications and technology, William Andrew, 2009.

[13]   S. Biira, B.A.B. Alawad, H. Bissett, J.T. Nel, T.P. Ntsoane, T.T. Hlatshwayo, P.L. Crouse, J.B. Malherbe, Influence of the substrate gas-inlet gap on the growth rate, morphology and microstructure of zirconium carbide films grown by chemical vapour deposition, Ceram. Int. 43 (2017) 1354–1361. doi:10.1016/j.ceramint.2016.10.092.

[14]   S. Biira, P.L. Crouse, H. Bissett, B.A.B. Alawad, T.T. Hlatshwayo, J.T. Nel, J.B. Malherbe, Optimisation of the synthesis of ZrC coatings in a radio frequency induction-heating chemical vapour deposition system using response surface methodology, Thin Solid Films. 624 (2017) 61–69. doi:10.1016/j.tsf.2017.01.018.

[15]   J. Park, T.S. Sudarshan, Chemical Vapor Deposition, ASM International, Chicago, 2001.

[16]   G.T. Farmer, J. Cook, Climate Change Science: A Modern Synthesis: Volume 1-The Physical Climate, Springer Science & Business Media, 2013.

[17]   Y. Zhu, L. Cheng, B. Ma, S. Gao, W. Feng, Y. Liu, L. Zhang, Calculation and synthesis of ZrC by CVD from ZrCl4–C3H6–H2–Ar system with high H2 percentage, Appl. Surf. Sci. 332 (2015) 591–598. doi:10.1016/j.apsusc.2015.01.175.

[18]   Y. Wang, Q. Liu, J. Liu, L. Zhang, L. Cheng, Deposition mechanism for chemical vapor deposition of zirconium carbide coatings, J. Am. Ceram. Soc. 91 (2008) 1249–1252. doi:10.1111/j.1551-2916.2007.02253.x.

[19]   J.H. Park, C.H. Jung, D.J. Kim, J.Y. Park, Temperature dependency of the LPCVD growth of ZrC with the ZrCl4-CH4-H2 system, Surf. Coatings Technol. 203 (2008) 324–328.

[20]   K.W. Woo, S.I. Yeo, Dalton's Law vs, Amagat's Law for the Mixture of Real Gases, (1995).

[21] X.-T. Yan, Y. Xu, Chemical vapour deposition: an integrated engineering design for advanced materials, 1st ed., Springer-verlag, London, 2010.

[22] R. Kossowsky, Surface Modeling Engineering, CRC Press, Florida, 1989.

[23] H.O. Pierson, Handbook of chemical vapor deposition: principles, technology and applications, William Andrew, New York, 1999. http://www.sciencedirect.com/science/article/pii/B9780815514329500061.

[24] M. Ohring, Materials science of thin films, 3rd ed., Academic press, London, 2002.

[25] M.S. Kim, J.S. Chun, Effects of the experimental conditions of chemical vapour deposition on a TiC/TiN double-layer coating, Thin Solid Films. 107 (1983) 129–139.

[26] Q. Liu, L. Zhang, L. Cheng, Y. Wang, Morphologies and growth mechanisms of zirconium carbide films by chemical vapor deposition, J. Coatings Technol. Res. 6 (2009) 269–273.

[27] Outotec, HSC Chemistry 7 (Thermo-chemical software), (2007).

[28] B.D. Cullity, S.R. Stock, Elements of X-ray Diffraction, 1st ed., Addison-Wesley Publishing company Inc, Massachusetts, 1956.

[29] J.P. Enríquez, X. Mathew, Influence of the thickness on structural, optical and electrical properties of chemical bath deposited CdS thin films, Sol. Energy Mater. Sol. Cells. 76 (2003) 313–322.

[30] C.-C. Liu, J.-H. Huang, C.-S. Ku, S.-J. Chiu, J. Ghatak, S. Brahma, C.-W. Liu, C.-P. Liu, K.-Y. Lo, Crystal Orientation Dynamics of Collective Zn dots before Preferential Nucleation, Sci. Rep. 5 (2015) 12533. doi:10.1038/srep12533.

[31] J.B. Nelson, D.P. Riley, An experimental investigation of extrapolation methods in the derivation of accurate unit-cell dimensions of crystals, Proc. Phys. Sciety. 57 (1945) 160–177.

[32] P. Schwarzkopf, R. Kieffer, F. Benesousky, Refractory hard metals: borides, carbides, nitrides and silicides, Macmillan, New York, 1953.

[33] E.K. Storms, The refractory carbides, Academic Press, New York, 1967.

[34] L. Toth, Transition metal carbides and nitrides, Academic press, New York, 1971.

[35] G.S. Schajer, Practical residual stress measurement methods, John Wiley & Sons, 2013.

[36] V.D. Mote, Y. Purushotham, B.N. Dole, Williamson-Hall analysis in estimation of lattice strain in nanometer-sized ZnO particles, J. Theor. Appl. Phys. 6 (2012) 1–8.

[37] M. Ermrich, D. Opper, XRD for the analyst: Getting acquainted with the principles, PANalytical, Eindhoven, 2013.

[38] S. Aksoy, Y.Y.Y. Caglar, S. Ilican, M. Caglar, Effect of deposition temperature on the crystalline structure and surface morphology of ZnO films deposited on p-Si, Adv. Control. Chem. Eng. Civ. Eng. Mech. Eng. (2010) 227–231.

[39] G.K. Williamson, R.E. Smallman, III. Dislocation densities in some annealed and cold-worked metals from measurements on the X-ray debye-scherrer spectrum, Philos. Mag. 1 (1956) 34–46.